AIAA JOURNAL
Vol. 45, No. 9, September 2007

Time–Frequency Analysis and Detection of Supersonic Inlet Buzz

Simon Trapier,* Sébastien Deck,† and Philippe Duveau†
ONERA, 92322 Châtillon, France
and
Pierre Sagaut‡
Université Pierre et Marie Curie, 75252 Paris, France

DOI: 10.2514/1.29196

Supersonic inlet buzz and, in particular, its onset were studied through the analysis of pressure records. These records are issued from an experimental study that was presented in a previous paper. The onset of buzz is a nonstationary phenomenon, and so the pressure signals could not be analyzed using classical signal-processing tools such as the Fourier transform, which does not take into account the possible evolutions in time. That is why time–frequency methods (spectrogram, wavelet transform, and Wigner–Ville distribution) were used. The evolution in time of the energy levels corresponding to buzz frequencies were studied. This analysis shows the existence of precursor phenomena that can appear several tenths of seconds before the onset of buzz. The detection of these precursors could, with the appropriate activation of a control device, allow the avoidance of buzz. Two change-detection algorithms (cumulative sum and generalized likelihood ratio) were tested on experimental pressure signals and proved their ability to successfully detect these precursors.

Nomenclature

$E(x)$	=	expectation of random variable x
f	=	frequency, Hz
h	=	detection algorithm threshold, dimensionless
K	=	ratio of standard deviations σ_1/σ_0, dimensionless
k	=	current (discrete) time, dimensionless
M	=	Mach number, dimensionless
prob(A)	=	probability of event A
$p_0(x)$	=	probability density function before change, Pa^{-1}
$p_1(x)$	=	probability density function after change, Pa^{-1}
S_k	=	cumulative sum of log-likelihood ratios, dimensionless
$S_x(t, f)$	=	short-time Fourier transform of signal $x(t)$
$SPW_x(t, f)$	=	smoothed pseudo-Wigner–Ville distribution of signal $x(t)$
s	=	wavelet scale factor, dimensionless
s_i	=	log-likelihood ratio, dimensionless
t	=	time, s
t_a	=	alarm time, s
$W_x(t, f)$	=	wavelet transform of signal $x(t)$
$WV_x(t, f)$	=	Wigner–Ville distribution of signal $x(t)$
x_k	=	discrete-time signal, Pa
$\hat{x}(f)$	=	Fourier transform of signal $x(t)$
$x(t)$	=	continuous-time signal, Pa
x^*	=	complex conjugate of x
Δf	=	frequency deviation, Hz
Δt	=	time deviation, s
η	=	mother-wavelet frequency, Hz
μ	=	mean of a Gaussian distribution
σ	=	standard deviation of a Gaussian distribution
σ_0	=	standard deviation of the signal before change, Pa
σ_1	=	standard deviation of the signal after change, Pa
τ	=	time translation, s
$\psi(t)$	=	mother wavelet
$\psi_{\tau,s}(t)$	=	wavelet of scale s, centered on time τ

Received 7 December 2006; revision received 4 May 2007; accepted for publication 10 May 2007.

*Ph.D. Student, Applied Aerodynamics Department.
†Research Scientist, Applied Aerodynamics Department.
‡Professor, Laboratoire de Modélisation pour la Mécanique.

I. Introduction

ALMOST every type of supersonic air inlet is subject to undesirable shock wave oscillations, commonly known as *inlet buzz*, which can lead to thrust loss, engine surge, or even structural damages. These instabilities arise when the entering mass flow is reduced below a given value known as the *buzz limit*. This phenomenon has been the subject of many studies, mainly experimental [1–5], since it was first observed by Oswatitsch in 1944 [6]. It is now well established that buzz is triggered by a shear layer (issued from the intersection point of normal and oblique shocks) entering the cowl lip (Ferri criterion) and/or a shock-induced separation developing on the compression surface that obstructs the inlet (Dailey criterion). Some attempts have been made to obtain theoretical models of this phenomenon [7–9], and a few numerical studies have also been conducted [10,11]. However, it is still impossible to predict the onset of buzz with sufficient precision.

Experiments on inlet buzz were conducted in 2004 in ONERA wind tunnel S3MA on a mixed-compression inlet model. The purpose of the experiments was to build a database and to improve the knowledge of buzz; the first results of that study are presented in [12]. Two kinds of shock oscillations were observed: *little buzz* and *big buzz*, which occurred at frequencies of around 120 and 18 Hz, respectively. The little buzz is thought to be due to an acoustic resonance phenomenon excited by the presence of a shear layer under the cowl lip, whereas the big buzz seems to be triggered by a boundary-layer separation on the compression ramps. Signal-processing analyses of unsteady pressure recordings showed that the big-buzz frequency was already present in the flow before the onset of large-amplitude shock oscillations, which suggested that the underlying mechanism of the big buzz, probably linked to acoustics, already exists before buzz starts.

In [12], emphasis was put on the analysis of the established self-sustained phenomenon. In this case, the pressure signals can be

considered as stationary in a statistical sense and classical nonparametric (periodogram) or parametric (autoregressive methods) signal-processing tools can be used. In the present paper, we focus on the short transient phase during buzz onset. The aforementioned spectral analysis methods are not adapted anymore, because the frequency content of the signal changes in time, and the Fourier transform (FT) does not explicitly take time into account. That is why we have to use more advanced signal-processing methods, which allow us to study the frequency content of a signal and its evolution in time.

Several tools exist that can be used for time–frequency analysis of nonstationary signals, such as the spectrogram, wavelet transform (WT), and Wigner–Ville distribution (WVD); they will be presented and their use will be discussed in Sec. III. Their application to our experimental pressure signals and the results obtained are also presented in that section.

One result of the time–frequency analysis of buzz-onset pressure signals is the existence of precursor phenomena that take place, in some cases, several tenths of seconds before buzz starts. If these precursors are detected early enough, a control device such as a variable ramp or a bypass door could be activated to avoid the onset of buzz (see [13] for an example of bypass doors that are activated in this amount of time). Indeed, although once buzz has started it cannot be easily controlled by simple methods, it could be possible to act before its onset (i.e., before the appearance of large separated areas and large-amplitude shock motions that make the phenomenon irreversible). It has been shown that simple control methods such as a bleed device [12] or a variable ramp [14] can efficiently delay the occurrence of buzz, which is why the ability to detect these precursors of buzz would be very interesting. However, the technical implementation of the possible control that would come after this detection is beyond the scope of this work. The issue of this detection by online algorithms is discussed in Sec. IV.

The purposes of the present paper are to show the existence of a precursor phenomenon before the onset of buzz using time–frequency analysis methods, to show that it is possible to automatically detect this precursor using the appropriate detection algorithms, and to introduce the methods used. Indeed, time–frequency analysis and detection algorithms (which are of common use in other domains, but almost unknown today in the field of aerodynamics) could, in our opinion, be very useful for many readers in their own works, which is why the description of the methods will occupy a relatively important place in the paper.

II. Experimental Setup and Results

This section briefly describes the setup of the experimental study and the data and results that were obtained. A more complete description can be found in [12].

A. Experimental Setup

Figure 1 shows a drawing of the inlet model, which is a mixed-compression supersonic inlet. About 85% of the compression is achieved by three external ramps and 15% is achieved by an internal convergent duct. The shock-on-lip Mach number is 2 (i.e., the Mach number for which the ramp shocks hit the lip). The inlet capture section is square-shaped with a 0.1×0.1 m^2 area. The inlet can be throttled by a butterfly-type valve located between the diffuser end and the mass flow meter. The total length of the duct between the cowl lip and the throttle is 1861 mm. The model could be equipped with or without bleed.

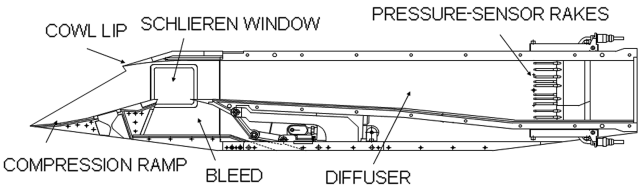

Fig. 1 Inlet model.

The inlet was richly equipped with steady and unsteady (Kulite) pressure sensors; its most upstream part, in particular, contained 30 Kulite sensors, the acquisition frequency of which was 10 kHz. Sensor rakes located in the diffuser allowed estimation of the pressure recovery of the inlet.

The model was tested for Mach numbers ranging from 1.8 to 3, with and without bleed. During each test, the throttle valve was initially open and so the inlet flow was stable. Then the entering mass flow, controlled by the valve, was progressively decreased until the buzz limit was reached. Unsteady pressure signals were recorded for 4 to 10 s when buzz started, then the valve was reopened until buzz stopped.

B. Experimental Results

In the present paper, we concentrate on the results obtained at $M = 1.8$ and 2. The flow patterns before and during buzz and the pressure signals recorded for these Mach numbers are presented hereafter.

1. Mach 1.8

The flow pattern just before the onset of buzz at Mach 1.8 is as shown in Fig. 2a. At this time, the inlet operates in the subcritical regime. A normal shock stands on the compression ramps, and the flow entering the inlet is subsonic. When the entering mass flow is reduced, the normal shock moves upstream until a separation appears at its foot. This separation obstructs the inlet section, and the entering mass flow strongly decreases. The shock is then expelled upstream and buzz begins. The shock oscillates between positions b (shock expelled upstream, almost up to the ramp tip) and position c (appearance of an internal normal shock, the flow looks like that in supercritical conditions), with a characteristic frequency of around 18 Hz. This low-frequency type of instability is referred to as the big buzz [4].

The pressure signal recorded by sensor PS33 (located in the diffuser) when the big buzz started is shown in Fig. 3; the pressure oscillations due to buzz can be clearly seen on it. This signal can be divided into three phases: before buzz, buzz onset, and buzz. The pressure signals recorded before buzz and during buzz are stationary in a statistical sense: their statistical properties are constant in time. These signals can be studied using classical signal-processing methods such as Fourier transform. Such a study was carried out and is presented in [12].

Focusing now on the transient phase during buzz onset, we observe that the pressure signals are nonstationary. The classical methods, which do not take into account any evolution in time, are

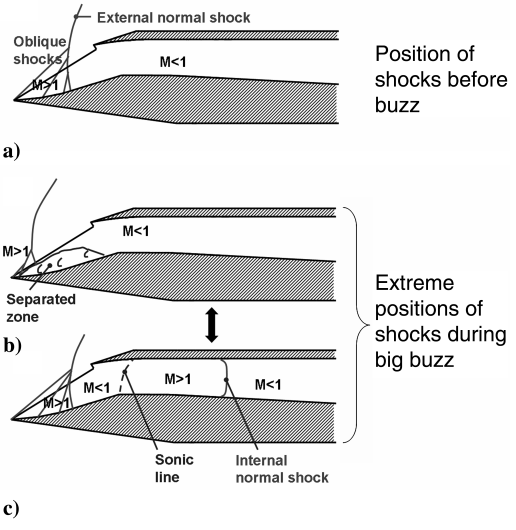

Fig. 2 Flow patterns before and during buzz at $M = 1.8$.

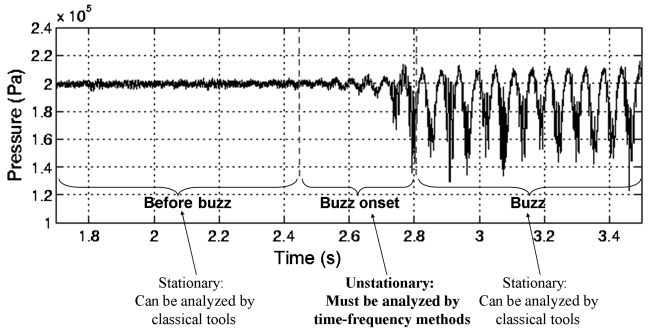

Fig. 3 Pressure signal recorded in the diffuser when the big buzz starts at $M = 1.8$.

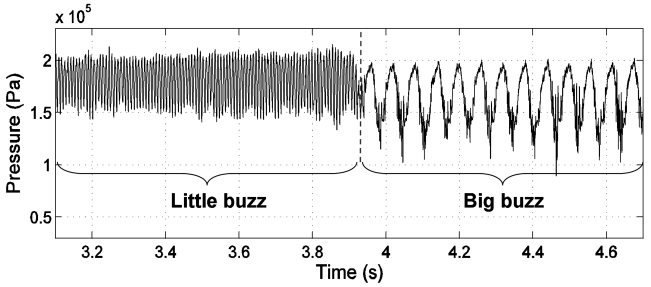

Fig. 4 Pressure signal recorded in the diffuser at the transition between the little and big buzz at$M = 2$.

then not relevant for the study of these signals; that is why time–frequency methods should be used, as described in Sec. III.

2. Mach 2

At $M = 2$ without bleed, when the entering mass flow is decreased from supercritical operation, as soon as the flow becomes subcritical, the little buzz arises. It consists of a shock oscillation that occurs at a frequency of around 120 Hz in our case. The shock motion has a much smaller amplitude than during the big buzz: the external shock remains on the third compression ramp, and the most downstream position of internal shock (when existing) is just behind the sonic line (see Fig. 2c). Contrary to the big buzz, no large separated area appears on the compression ramps.

Although the little buzz seems to be less violent than the big buzz, the amplitude of the pressure fluctuations inside the inlet is quite the same. When mass flow is further reduced, the little buzz stops and is immediately replaced by the big buzz (see Fig. 4), which is similar to that already described at $M = 1.8$.

The little buzz is thought to be a phenomenon of acoustic resonance (its frequency is an acoustic resonance mode of the inlet), which is excited by the presence of shear layers passing under the cowl lip. The shear layers are issued from the intersection between the oblique shocks generated by the compression ramps and the external normal shock. For a more detailed description of this phenomenon, one may refer to [12].

An interesting fact about the little buzz is that it can be virtually suppressed by introduction of a bleed device. Indeed, the bleed stabilizes the internal shock and damps the internal pressure oscillations, and so the resonance phenomenon that generates the little buzz cannot occur. On the other hand, the big buzz can not be suppressed by the bleed.

III. Time–Frequency Analysis

A nonstationary signal is a signal for which the statistical properties (such as mean, variance, spectral content, etc.) change in time. This kind of signal has to be studied using spectral descriptions that are functions of both time and frequency. Several tools have been developed to perform this type of analysis, such as the spectrogram, wavelet transform, and Wigner–Ville distribution. In the field of aerodynamics, these methods (in particular, wavelet transform) have already been used on experimental signals [15–17] for the study of turbulent flow or acoustics [18], as well as on signals from numerical simulations [19]. These methods are briefly presented hereafter and the reader interested in their theoretical background is referred to [20–23].

A. Theoretical Presentation

1. Short-Time Fourier Transform

a. Definition. To design a time–frequency analysis tool, the more intuitive idea is not to apply the FT to a whole signal $x(t)$, but to apply the FT to a windowed part of the signal that is of finite duration.

Let $g(t)$ be a short-time window localized around $t = 0$. The Fourier analysis of $x(t) \cdot g(t - \tau)$ will allow the study of the spectral content of $x(t)$ around τ.

The short-time Fourier transform (STFT) is defined as

$$Sx(\tau, f) = \int_{-\infty}^{+\infty} x(t) g(t - \tau) \cdot e^{-2i\pi f t} \, \mathrm{d}t \tag{1}$$

The STFT gives a representation of $x(t)$, which is a function of both time and frequency. Its squared modulus $|Sx(t, f)|^2$ is an energy density (expressed in $\mathrm{Pa}^2/\mathrm{s} \cdot \mathrm{Hz}$). The plot of $|Sx(t, f)|^2$ is called a spectrogram; it is a two-dimensional time–frequency representation of signal $x(t)$.

b. Time–Frequency Atoms. The STFT can be expressed as the Fourier transform of the windowed signal $x(t) \cdot g(t - \tau)$, but it can also be considered as the scalar product of $x(t)$ with the modulated window $g(t - \tau) \cdot e^{2i\pi f t}$. The function $g(t - \tau) \cdot e^{2i\pi f t}$ is called a *time–frequency atom*, because it is localized around a particular time τ and a given frequency f, and it allows the study of $x(t)$ at the given time and frequency.

An atom of finite and nonzero duration cannot be perfectly localized both in time and frequency. It is necessarily spread around a mean time τ, and its Fourier transform is spread around a mean frequency f. Then its time and frequency deviations Δt and Δf can be defined around these mean values. The *time–frequency localization* of an atom is represented as a *Heisenberg box*, which is a rectangle of time width Δt and frequency height Δf, located in the time–frequency plane (see Fig. 5, left).

The values Δt and Δf determine the spectrogram resolution. For instance, the higher the Δf value, the more the time–frequency atom is spread around f and thus does not allow a precise analysis of the signal at this particular frequency, and so the frequency resolution of the spectrogram will be poor in this case; Δt has a similar role for time resolution.

A property of these deviations is that they follow the rule of $\Delta t \cdot \Delta f = \text{const}$. This rule is known as the uncertainty theorem of Heisenberg; it means that no time–frequency atom can be perfectly localized both in time and frequency. It also means that the time resolution of a spectrogram cannot be increased without lowering the frequency resolution and vice versa. A compromise between time and frequency resolution must therefore be done. The important parameter here is the window length: a short window allows good precision in time, but poor precision in frequency. A long window means good precision in frequency, but results in poor localization in time.

2. Wavelet Transform

Wavelet transform (WT) is another time–frequency representation that also uses time–frequency atoms. Instead of modulated windows, these time frequencies atoms are wavelets. A wavelet is a function $\psi(t)$ with a zero mean and finite energy.

Given a wavelet ψ, called the mother wavelet, a wavelet family $\psi_{\tau,s}$ can be derived as

$$\psi_{\tau,s}(t) = \frac{1}{\sqrt{s}} \psi\left(\frac{t - \tau}{s}\right) \tag{2}$$

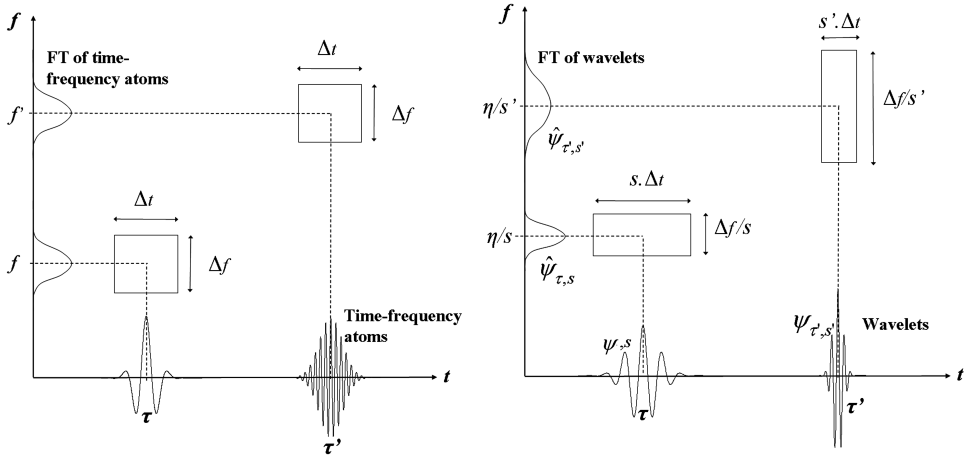

Fig. 5 Heisenberg boxes of two frequency atoms used for STFT (left) and WT (right).

The wavelets $\psi_{\tau,s}$ are obtained by translations and dilatations of the mother wavelet, where τ is the time translation parameter, and s is the timescale dilatation parameter.

The wavelet transform $Wx(\tau, s)$ of a signal $x(t)$ is defined as

$$Wx(\tau, s) = \int_{-\infty}^{+\infty} x(t) \frac{1}{\sqrt{s}} \psi^* \left(\frac{t-\tau}{s} \right) \mathrm{d}t \tag{3}$$

where * stands for the complex conjugate, and Wx is complex (the plot of its squared modulus $|Wx(\tau, s)|^2$ is called a scalogram: it is not a time–frequency representation, but a timescale representation). However, it is possible to link the scale factor s to a frequency. Indeed, if the mother wavelet is a time–frequency atom localized around time $t = 0$ and frequency η, then the dilated and translated wavelet $\psi_{\tau,s}$ is a time–frequency atom localized around time τ and frequency η/s. So a scalogram in the plane (τ, s) can be considered as a time–frequency representation in the plane (t, f), with $t = \tau$ and $f = \eta/s$.

The main property of wavelets is that they are time–frequency atoms with a variable length, and so their time and frequency deviations are not constant and they can be adapted to the phenomenon that has to be studied, similar to using a microscope. At high frequencies, the studied phenomena have a short duration and one will use wavelets with a low scale factor s, and so the time resolution is good. Conversely, at low frequencies, one will rather use wavelets with a high scale factor s to have a good precision in frequency.

Figure 5 (right) shows the Heisenberg boxes of two wavelets having different scale factors s and s'. It can be seen that the proportions of those Heisenberg boxes are not the same, whereas their area $\Delta t \cdot \Delta f$ is the same. It can be noted that the Heisenberg theorem is still valid. This adaptability of resolution to the studied frequency is the main advantage of the scalogram in comparison with the spectrogram.

Many types of wavelets exist and are used for different purposes. In the present paper, we will use the Gabor wavelet, which is defined by

$$\psi(t) = \frac{1}{(\sigma^2 \pi)^{1/4}} e^{\left(\frac{-t^2}{2\sigma^2}\right)} e^{i\eta t} \tag{4}$$

where σ and η are two parameters allowing control of, respectively, the time dispersion and the frequency of the mother wavelet.

3. Wigner–Ville Distribution

Unlike the spectrogram or scalogram, which belong to the family of atomic decompositions, the WVD is a quadratic distribution that depends directly on time and frequency. The WVD of a signal $x(t)$ is defined by

$$WV_x(t, f) = \int_{-\infty}^{+\infty} x\left(t + \frac{\tau}{2}\right) x^*\left(t - \frac{\tau}{2}\right) e^{-2i\pi\tau f} \, \mathrm{d}\tau \tag{5}$$

Unlike the STFT and the WT, the WVD is real-valued; like the spectrogram and scalogram, it has the dimensions of an energy density. It belongs to the family of quadratic distributions. It does not use time–frequency atoms and so it is not concerned with the Heisenberg theorem, as expressed earlier. However, it still remains an uncertainty problem, due to the existence of cross terms issued from the quadratic nature of the distribution. Indeed, the WVD of the sum of two signals is not the sum of the WVD of these signals. This results in the fact that two frequencies f_1 and f_2 will create an interference frequency $(f_1 + f_2)/2$. This frequency, not actually present in the signal, will appear on the WVD representation and make its interpretation difficult. However, these confusing cross terms can be damped by the use of a smoothing window $\Pi(t, f)$:

$$SPW_x(t, f) = \int_{+\infty}^{-\infty} \int_{+\infty}^{-\infty} \Pi(\tau - t, \xi - f) WV_x(\tau, \xi) \, \mathrm{d}\tau \, \mathrm{d}\xi \tag{6}$$

where $\Pi(t, f) = \hat{h}(-f) g(t)$ and $h(t)$ and $g(t)$ are two windows (rectangular, Hamming, etc.); $\hat{h}(f)$ denotes the Fourier transform of $h(t)$; and if $x(t)$ is in pascal, then $|S_x(t, f)|^2$, $|W_x(t, f)|^2$, $|WV_x(t, f)|$, and $|SPW_x(t, f)|$ are in $\mathrm{Pa}^2 \cdot \mathrm{s}^{-1} \cdot \mathrm{Hz}^{-1}$. This new distribution is called the *smoothed pseudo-Wigner–Ville distribution* (SPWVD).

The previous compromise of the spectrogram and scalogram between time and frequency resolutions is replaced here by a compromise between the time–frequency resolution and the interference level: the more one smoothes in time and/or frequency, the poorer the resolution in time and/or frequency will be (for further discussion, see [20]).

B. Analysis of Buzz Signals

1. Time–Frequency Representations of an Example of the Experimental Signal

This section compares the representations provided by the three methods previously described (spectrogram, scalogram, and SPWVD) for an example of the experimental signal. The signal that is to be studied with these methods should have a zero mean, which is why, before analyzing it, one should subtract its running average from the signal so that it is centered on zero, but without changing its fluctuations. This is equivalent to cutting all frequencies lower than the frequencies of the studied fluctuations. In our case, this cutting frequency will be 10 Hz (the big-buzz frequency is 18 Hz).

Figure 6 shows a spectrogram, a scalogram, and a smoothed pseudo-Wigner–Ville distribution for the same signal; this signal has already been presented in Fig. 3 (it was recorded in the diffuser when the big buzz started at $M = 1.8$).

The parameters of each representation were tuned to give the best results:

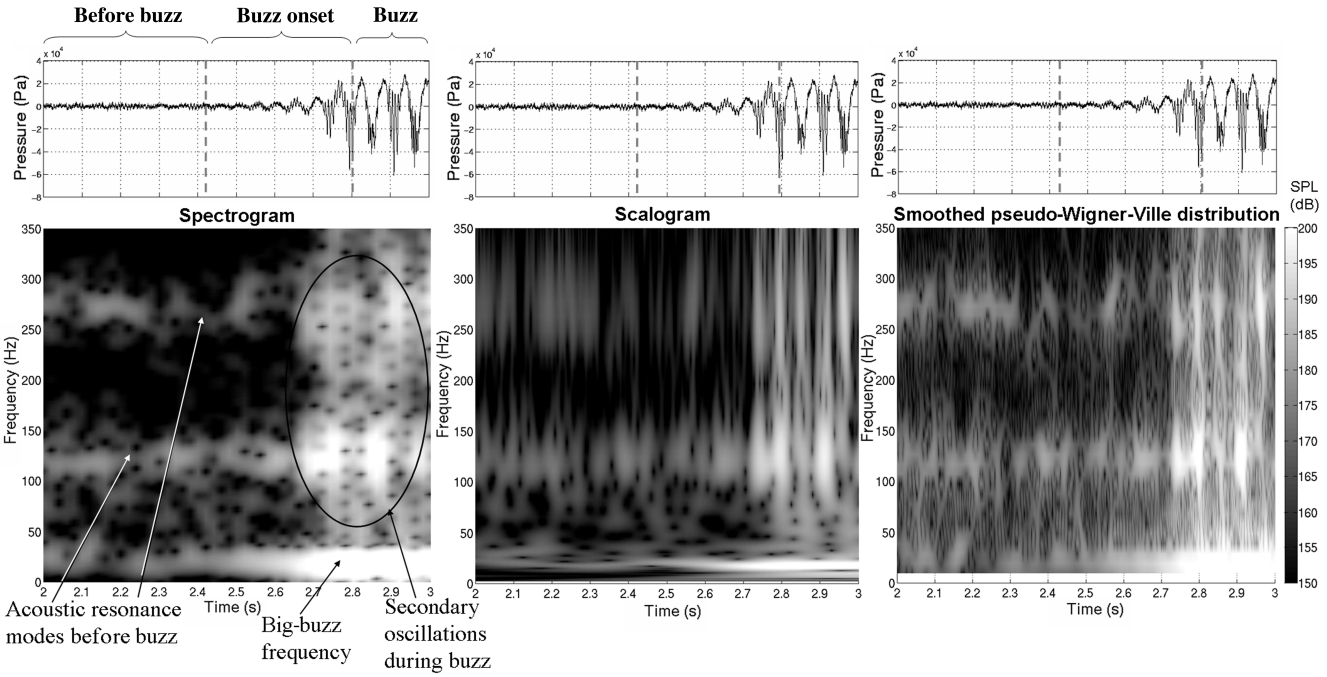

Fig. 6 Spectrogram, scalogram, and SPWVD of a pressure signal.

1) For the spectrogram, the sliding window length is 0.1 s. After several tests, this value appeared to give the best compromise between time and frequency in terms of resolution. A shorter window resulted in a poor precision in time, whereas a longer window made the different frequencies difficult to separate.

2) For the scalogram, the parameters of the Gabor wavelet are $\sigma^2 = 0.5$ and $\eta = 15$ Hz [see Eq. (4)]; σ^2 has a similar role to window length for a spectrogram and it was chosen to give a quite good precision at low frequencies (and in particular buzz frequency) without debasing the precision in time; η is the mother-wavelet frequency and if it is too small (lower than 5 Hz), the frequency resolution will be poor, but it has no important effect when higher than 15 Hz.

3) For the SPWVD, the time resolution (length of the time-smoothing window g) is 2×10^{-2} s and the frequency resolution (inverse of the length of the frequency-smoothing window h) is 10 Hz. These values provide acceptable resolutions in time and frequency, while damping the interferences enough to make the SPWVD easily readable.

The physical meaning of the different elements appearing in Fig. 6 will be detailed in the next section. Among the three representations, the spectrogram shows the poorest resolution with the retained parameters. The SPWVD and the scalogram allow a better precision. The adaptable resolution of the scalogram clearly appears here: the highest frequencies are badly resolved, whereas the lowest frequencies are accurately predicted. The buzz frequency, in particular, appears as a thin line instead of the wide stripe seen in the spectrogram and SPWVD.

Because this low frequency is the frequency of interest in this study, the scalogram is the most relevant tool and will be used in the following sections (with the same parameters as in the present section).

2. *Mach 1.8: Big Buzz*

This section focuses on the signature of pressure signals before the big buzz at $M = 1.8$. We get interested in the pressure signal recorded at the beginning of buzz, during the transition between stable flow and buzz.

The plots in Fig. 6 show the different frequencies existing in the signal recorded in the diffuser before and during buzz, as well as their evolution. The three representations have the same global appearance. Before buzz, they show horizontal stripes for frequencies of around 120, 270, and 430 Hz. These stripes correspond to low-amplitude fluctuations of pressure that have already been described in [12] and are linked to acoustic resonance modes of the inlet. When the big buzz begins, a horizontal stripe at its frequency (18 Hz) appears, at a much higher level of energy. Higher-frequency *spots* can also be seen; they correspond to *secondary oscillations* that occur during buzz [12]. They appear as spots and not as stripes, because these oscillations only take place during a part of the buzz cycles when the normal shock is expelled upstream, and they disappear when the flow resembles that in supercritical conditions (shock swallowed).

It can be seen on these plots that the big-buzz frequency (18 Hz) is already present before buzz onset, which occurs at around $t = 2.78$ s. This frequency does not appear bluntly in the signal, but grows progressively, over several tenths of seconds.

It is possible to plot the energy level of this particular frequency against time (i.e., a "slice" of the wavelet transform at this frequency), which allows visualizing the evolution of its energy level more clearly. Such a plot is shown in Fig. 7 for the signals recorded by sensors K19 (located on the compression ramps, just upstream of the normal shock before buzz), K2 (over the compression ramps, just downstream of the normal shock before buzz), and PS33 (located in the diffuser).

Figure 7 shows that the energy at buzz frequency begins to grow at around $t = 2.45$ s (i.e., 0.3 s before buzz starts). This progressive

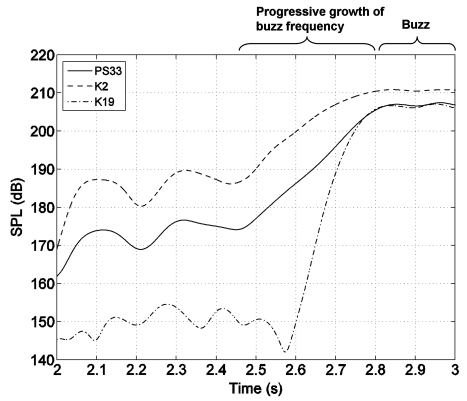

Fig. 7 Energy levels of pressure signals PS33, K19, and K2 at frequency 18 Hz at $M = 1.8$.

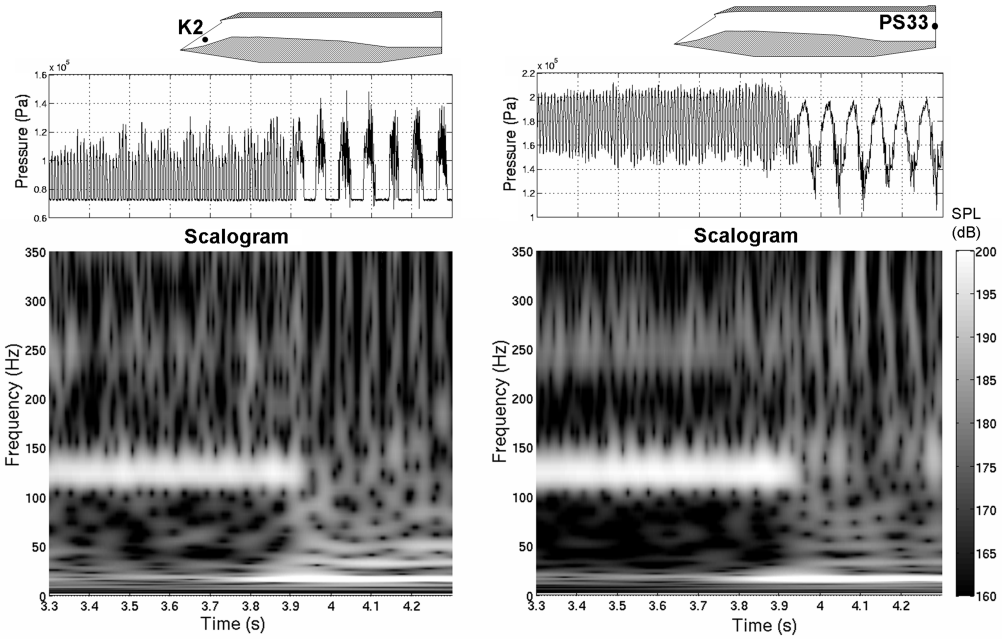

Fig. 8 Scalograms of the signals recorded at transition between the little buzz and the big buzz at $M = 2$ without bleed.

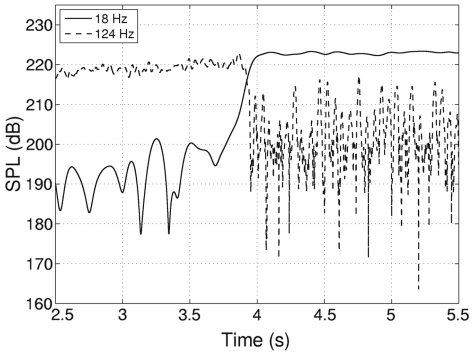

Fig. 9 Energy levels at frequencies 18 and 124 Hz for sensor PS33 at $M = 2$ without bleed.

growth is visible on the signal of every sensor located downstream of the shock before buzz (here, K2 and PS33). On the other hand, this growth is more abrupt for K19, which is located upstream of the normal shock before the onset of buzz and is therefore not affected by the oscillations of the internal pressure before buzz.

3. Mach 2: Little Buzz and Big Buzz

a. Without Bleed. Figure 8 shows the wavelet transforms of pressure signals recorded by sensors K2 (located over the second compression ramp) and PS33 (diffuser) at the transition between the little buzz and the big buzz.

The little buzz appears as a horizontal stripe at around 120 Hz. Its first harmonic at 240 Hz is also visible; at $t = 3.9$ s, it disappears and is replaced by the big buzz. However, even during the little buzz, the big-buzz frequency is already present in the signal, which cannot be directly seen on the signals, because the oscillations at 18 Hz are hidden by those of the little buzz. Just as at $M = 1.8$, the big-buzz frequency appears progressively in the signal over several tenths of seconds, while the little buzz is still prevailing.

Figure 9 shows the energy levels against time at frequencies of 18 Hz (big buzz) and 124 Hz (little buzz) for sensor PS33, in which the progressive increase of the energy level of the frequency of 18 Hz can be seen. One can also see that the energy seems to switch from 124 to 18 Hz (from the little buzz to the big buzz) and that the total energy remains constant.

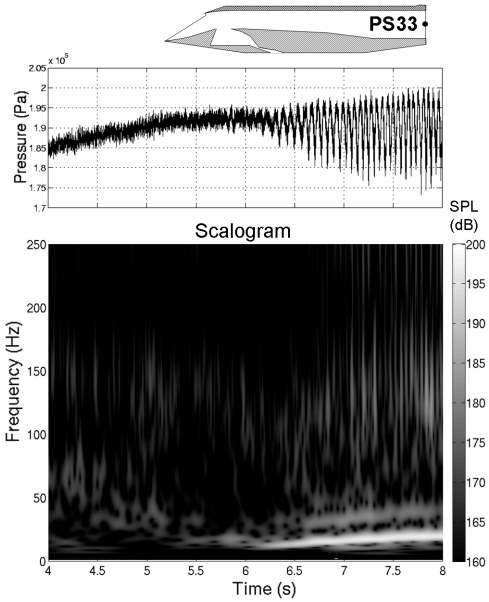

Fig. 10 Scalogram of the signal recorded at $M = 2$ with bleed.

b. With Bleed. The wavelet transforms of the pressure signal recorded by sensor PS33 (diffuser) at the beginning of the big buzz at $M = 2$ with bleed is shown in Fig. 10. The energy levels at frequencies 18 and 124 Hz for the same sensor are plotted in Fig. 11, in which the following can be observed:

1) The little buzz is suppressed by the bleed. Before the big buzz occurs, no particular frequency appears, only broadband noise due to bleed cavity flow. This suppression of the little buzz had already been noticed and mentioned in [12] and is due to the fact that bleed stabilizes the internal shock and damps its oscillations.

2) The growth of the energy level of frequency 18 Hz when the big buzz arises occurs very softly. The bleed tends to smooth all phenomena, including the big buzz start.

C. Usefulness for the Detection of Buzz Onset

The main result provided by the time–frequency analysis is that in every case studied, before the beginning of the big buzz, there was a phase during which the energy level at the big-buzz frequency grew

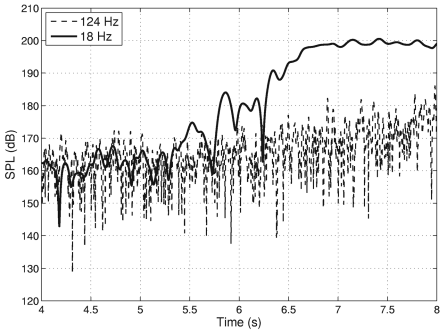

Fig. 11 Energy levels at frequencies 18 Hz and 124 Hz for sensor PS33 at $M = 2$ with bleed.

progressively in the pressure signals. This growth of the energy level, which lasted several tenths of seconds, is a precursor phenomenon that heralds the onset of the big buzz.

If this precursor can be automatically detected online early enough, a control device such as a variable ramp or a bypass door could be activated to avoid the onset of buzz. Indeed, control by simple methods, although difficult once buzz has started, can be efficient if activated before large separated areas and shock oscillations have developed and made the phenomenon irreversible (i.e., before buzz onset).

The ability to detect this precursor online, which is indicated by a change in the properties of pressure signals, is therefore important. This detection can be achieved using a change-detection algorithm, as described in the next section.

IV. Detection of Buzz Onset: Change-Detection Algorithms

Change detection in a signal is an issue that can be found in a wide range of domains including aerodynamics [24], speech analysis, seismology, or medicine [25]. Many detection algorithms that are adapted to those various applications have been developed. This section presents the change-detection algorithms that should be used to detect the presence of buzz precursors online: namely, the cumulative sum (CUSUM) and generalized likelihood ratio (GLR) algorithms. The major interest of these algorithms (in comparison with a simple control of RMS levels, for instance) is that they take into account the history of the signal (i.e., the duration of the change) and its amplitude. For a complete presentation of this field and of the other existing algorithms, one may refer to [26]. We will first briefly introduce the theoretical concepts upon which these algorithms are based.

A. Statistical Properties of Random Signals

1. Probability Density Function

The pressure signals that we have to study are random signals; their value $x(t)$ at a given time t is a random variable. One important property of such a signal is its probability density function (PDF), which can be defined and estimated, from an engineering point of view, in terms of relative frequency of occurrence [27].

The probability density functions of experimental random variables are often approximately Gaussian when the value of the random variable depends on a large number of independent effects. The Gaussian distribution is defined by

$$p(x) = \frac{1}{\sqrt{2\pi}\sigma} e^{-\frac{(x-\mu)^2}{2\sigma^2}} \tag{7}$$

where μ is the mean and σ^2 is the variance of the Gaussian distribution (σ is also called the *standard deviation* of the distribution).

It can be seen in the examples of Fig. 12 (right) that the PDFs of our experimental signals are nearly Gaussian. At this stage, it is also useful to introduce the expectation of a continuous random variable x, defined by

$$E(x) = \int_{-\infty}^{+\infty} x \cdot p(x)\,\mathrm{d}x \tag{8}$$

where $p(x)$ is the probability density function of x. If $x(t)$ is a random signal, the expectation of $x(t)$ is simply the mean of the signal.

2. Likelihood Ratio Test

The likelihood ratio test is a statistical test that is used by the change-detection algorithms that will be introduced later. If $p_0(x)$ and $p_1(x)$ are two probability density functions, then this test allows us to determine from one observed value x_i of a random variable whether that variable is more likely to follow the PDF $p_0(x)$ or $p_1(x)$. This test uses the log-likelihood ratio defined by

$$s(x_i) = \ell_n \frac{p_1(x_i)}{p_0(x_i)} \tag{9}$$

This ratio compares the PDFs $p_0(x)$ and $p_1(x)$ at the observed value x_i. Note that $s(x_i)$ is positive when $p_0(x_i) < p_1(x_i)$ and negative when $p_0(x_i) > p_1(x_i)$.

Let x be a random variable; $s(x)$ is then a random variable with the following properties:

1) If x follows the probability density $p_0(x)$, then the expectation of $s(x)$ will be negative: $E[s(x)] < 0$.

2) If x follows the probability density $p_1(x)$, then the expectation of $s(x)$ will be positive: $E[s(x)] > 0$.

This property is used by the algorithms CUSUM and GLR.

B. CUSUM Algorithm

1. Theory

The cumulative sum algorithm [28] is one of the most commonly used in change detection. It can only be used if the nature of the change in the signal is known. More exactly, the properties of the signal after change must be known in advance. This is possible in our

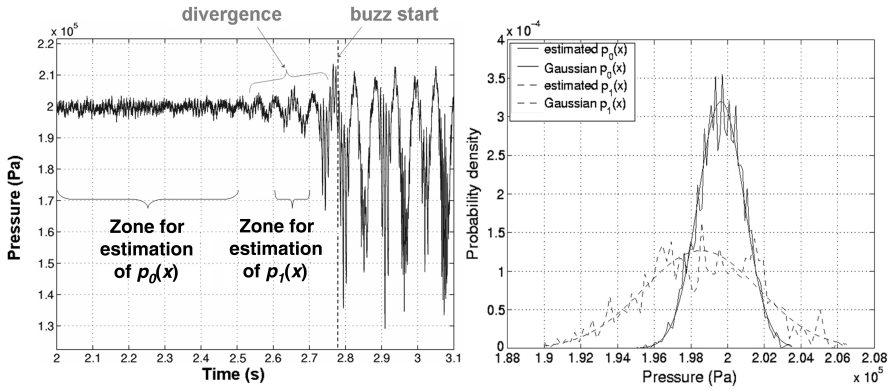

Fig. 12 Signal PS33 at beginning of buzz (left), and estimations of PDFs $p_0(x)$ and $p_1(x)$ (right).

case, with some hypotheses that have to be made and that will be described later.

The CUSUM algorithm detects a change in the probability density of the analyzed signal. The probability densities before change $p_0(x)$ and after change $p_1(x)$ are supposed to be known. The analyzed signal is a series of measured values x_i $(i = 1 \ldots k)$, where x_k denotes the last (i.e., the most recent) recorded point.

Let s_i be the log-likelihood ratio of the probability densities before and after change $p_0(x)$ and $p_1(x)$:

$$s_i = \ell_n \frac{p_1(x_i)}{p_0(x_i)} \tag{10}$$

Let S_k be the cumulative sum of these ratios for all points recorded so far:

$$S_k = \sum_{i=1}^{k} s_i \tag{11}$$

Let m_k be the minimum value that was reached by S_k:

$$m_k = \min_{1 \le j \le k} S_j \tag{12}$$

The algorithm compares S_k to its minimum value m_k and detects a change (and gives the alarm) at time t_a if their difference is greater than a user-defined threshold h:

$$t_a = \min(k | S_k - m_k \ge h) \tag{13}$$

As long as the signal follows the probability density $p_0(x)$, the expectation of s_i is negative and so S_k is decreasing. But as soon as the signal probability density is changed into $p_1(x)$, the expectation of s_i becomes positive and S_k increases. When the difference between S_k and its minimum m_k reaches the threshold h, the alarm is given (see the example in Fig. 13).

The parameter h allows the user to adjust the algorithm sensibility. For low h values, the algorithm will be able to detect small changes or to quickly detect bigger changes. On the other hand, a low h value increases the risk of false alarm. Conversely, the algorithm with high h is safer, but delays the detection of a change. The choice of h is therefore very important and strongly influences the algorithm performance. The appropriate choice of this threshold value will be discussed in Sec. IV.B.4.

2. *Application to Buzz Detection*

Figure 12 (left) shows the signal of sensor PS33 (located in the diffuser), recorded when the big buzz started at $M = 1.8$. One can see the progressive divergence of the oscillations at 18 Hz, already described. This divergence is the change that is to be detected and it is translated into an increase in variance of the PDF of the signal. It is possible to estimate the probability densities of the signal before and after change and to approximate them with Gaussian distributions (Fig. 12, right); these Gaussians will be used by the CUSUM algorithm in the determination of the log-likelihood ratio.

The algorithm can then be run, as described in Sec. IV.B.1. Figure 13 shows the evolution of the series S_k and the alarm time, with a threshold value of $h = 100$; with this parameter, the alarm time is $t_a = 2.584$ s.

We consider that buzz has irreversibly started when the normal shock has reached the most upstream compression ramp for the first time and when a large separation has appeared at its foot. This happens in the present case at $t = 2.78$ s, and so the algorithm gives the alarm almost 0.2 s before buzz starts.

The algorithm exhibits rather good performances here, but in quite an unrealistic case. Of course, in a real situation, it is impossible to know the exact probability density functions $p_0(x)$ and $p_1(x)$ in advance. Other problems may also appear: First, what is to be detected is an increase in variance, but a change in mean could also occur and is likely to set off the alarm when it should not. Another problem is that noise in the signal could make an increase in the amplitude of the frequency of interest (around 18 Hz) difficult to detect. To overcome these difficulties, adaptations in the algorithm are required.

3. *Adaptations of the Algorithm*

Before applying the detection algorithm to our signal, the latter has to be preprocessed, as shown in Fig. 14. First, to solve the problem of the variation of mean, one should use a running average, as described in Sec. III.B.1, so that the mean of the signal is constant and equal to zero. Concerning the problem of noise, a solution consists of filtering the signal using a low-pass filter that cuts the highest frequencies.

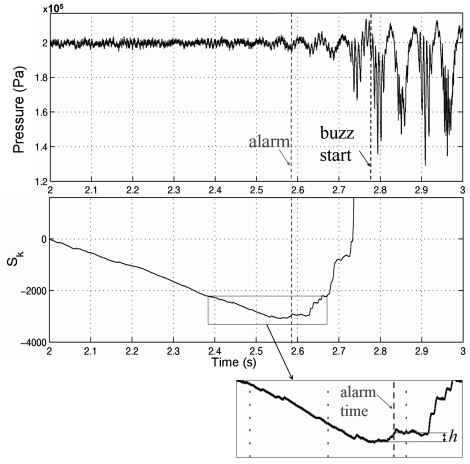

Fig. 13 Detection of the signal PS33 divergence at $M = 1.8$ by the CUSUM algorithm.

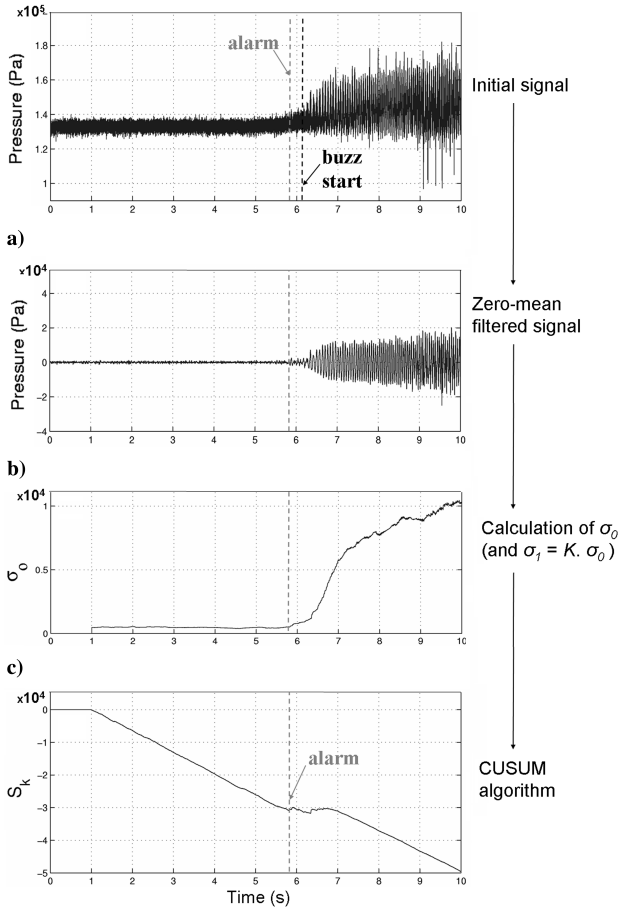

Fig. 14 Detection of the big buzz onset on signal K6 at $M = 2$ with bleed by the CUSUM algorithm.

Figure 14a shows the signal of sensor K6 (located on the sidewall over the compression ramps) at $M = 2$ with bleed. Figure 14b shows the same signal, after subtraction of its running average and filtering. The filter cutting frequency is 70 Hz. One can see that the signal mean is now constant and that the divergence of the 18-Hz oscillations appears much more clearly after filtering, thus making it easier for the algorithm to detect them. The pressure signals should be processed in this way (online) before using the algorithm.

The CUSUM algorithm also needs the probability densities before and after change: $p_0(x)$ and $p_1(x)$. They will be considered as Gaussian distributions, because we saw that this distribution gives a good approximation of the real PDF of the signal. A Gaussian distribution is defined by two parameters: its mean μ and its standard deviation σ. After subtraction of their running average, our signals have a zero mean, and so $\mu = 0$ for $p_0(x)$ and for $p_1(x)$.

Finally, the parameters that we have to supply to the algorithm are the standard deviations of $p_0(x)$ and $p_1(x)$, which will be called, respectively, σ_0 and σ_1, where σ_0 is the standard deviation of the signal before change. We choose to take the standard deviation of the signal for σ_0, estimated online between t-Δt and t, where t is the current time and Δt is a window length. The value of Δt should be long in comparison with the timescale of the phenomenon to detect, so that the calculated σ_0 is not affected by short insignificant variations in the signal; we took it equal to 0.5 s, which is approximately the duration of ten buzz cycles.

The algorithm has to detect a divergence (i.e., an increase in the standard deviation), and so σ_1 has to be greater than σ_0. We will therefore use for σ_1 the value of σ_0 that was calculated, multiplied by a coefficient $K > 1$: $\sigma_1 = K \cdot \sigma_0$. K becomes a new parameter of the algorithm, and its effect is similar to h: the smaller K, the more sensitive the algorithm; its value has to be experimentally determined. In the present case, we found an optimal value of around 3 for K. This value of 3 approximately corresponds to the average increase in standard deviation that was observed in our experimental cases; it is, for instance, the ratio between the standard deviations of $p_0(x)$ and $p_1(x)$ in Fig. 12.

Figure 14 sums up all of the steps of a change detection using this modified version of the CUSUM algorithm: subtraction of running average and filtering, calculation of the standard deviations σ_0 andσ_1, calculation of the series S_k, and alarm. In this example, the window length for the calculation of σ_0 was $\Delta t = 0.5$ s, the coefficient K was taken equal to three, and the threshold was $h = 400$ (see the following section). The alarm time given by the algorithm is $t_a = 5.829$, more than 0.3 s before buzz starts.

One can note that the continuous decrease of the series S_k can lead it to reach very low values when analyzing a long real signal online. To overcome this difficulty, one can define S_k differently, in the following way:

$$\text{if } S_{k-1} + s_k > 0 \quad \text{then } S_k = S_{k-1} + s_k \quad \text{else } S_k = 0 \tag{14}$$

With this recursive definition, when S_k is not increasing, it remains positive; the rest of the algorithm does not change.

4. Choice of Threshold h

The choice of threshold h is very important: it has to be great enough to avoid (or to at least minimize) the risk of false alarm, but small enough for the algorithm to remain sensible. The best way is to adjust it by trying several values on a given experimental signal, if available. However, we propose a value that should be efficient, in most cases, for this particular situation: detection of a change in variance of a zero-mean Gaussian distribution, which depends on the ratio between the standard deviations after and before change ($K = \sigma_1/\sigma_0$).

In this particular situation [$p_0(x)$ and $p_1(x)$ are zero-mean Gaussians], the log-likelihood ratio is

$$s_i = \ell_n \frac{p_1(x_i)}{p_0(x_i)} = \ell_n \left(\frac{\sigma_0}{\sigma_1}\right) + \left(\frac{x_i^2}{2\sigma_0^2} - \frac{x_i^2}{2\sigma_1^2}\right) \tag{15}$$

After the change, assuming that the variance of x_i is σ_1^2, the expectation of x_i^2 will be $E(x_i^2) = \sigma_1^2$ and the expectation of s_i will be

$$E(s_i) = -\ell_n K + \frac{K^2}{2} - \frac{1}{2} \tag{16}$$

where $K = \sigma_1/\sigma_0$.

If the variance of the analyzed signal changes from σ_0^2 to σ_1^2 at a time of k_1, the average increase of

$$S_k = \sum_{i=1}^{k} s_i$$

between k_1 and $k_2 > k_1$ will be

$$E(S_{k2} - S_{k1}) = (k_2 - k_1) \cdot \left(-\ell_n K + \frac{K^2}{2} - \frac{1}{2}\right) \tag{17}$$

We propose the following semi-empirical rule for the choice of threshold h:

$$h = 0.25 \frac{f_S}{f_B} \left(-\ell_n K + \frac{K^2}{2} - \frac{1}{2}\right) \tag{18}$$

where f_B is the frequency of buzz (18 Hz in the present case), and f_S is the sampling frequency of the signal (10,000 Hz for our signals).

This value of h ensures, in the ideal case, that the alarm is given when the variance of the signal has changed from σ_0^2 to σ_1^2 for a time that is equivalent to a quarter of a buzz period (this coefficient of 0.25 is purely empirical). This value of h has proven to be efficient for our signals.

However, the value of h and other parameters (K, in particular) has to be tested on at least one real signal to be precisely tuned. For that purpose, a wind-tunnel experimental study of the inlet is probably necessary.

To evaluate the sensibility of the algorithm to the threshold, Table 1 shows the alarm time for different values of h, from 100 to 1500, for the signal of Fig. 14 [the value provided by Eq. (18) is $h = 400$]. The buzz start time was around $t = 6.2$ s. The alarm time is correct when h is in a range from 200 to 1000.

C. GLR Algorithm

1. Theory

The CUSUM algorithm appears to be an efficient tool to detect inlet buzz, but needs information about the state after the change that the algorithm is supposed to detect. Contrary to the CUSUM algorithm, the GLR algorithm [29] does not need the knowledge of the PDF after change; its principle is the following:

The PDFs before and after change [$p_0(x)$ and $p_1(x)$] are supposed to depend on a parameter θ; the variation of this parameter is to be detected. The PDFs can be called $p_{\theta_0}(x)$ and $p_{\theta_1}(x)$, where θ_0 and θ_1 are the values of θ before and after change.

The GLR and CUSUM algorithms use the sum of log-likelihood ratios:

$$S_j^k(\theta_1) = \sum_{i=j}^{k} \ell_n \frac{p_{\theta 1}(x_i)}{p_{\theta_0}(x_i)} \tag{19}$$

Table 1 Alarm times for different threshold values; buzz start time was around $t = 6.2$ s

h	100	200	400	500	1000	1500
Alarm time t_a	1.560 s (false alarm)	5.825 s	5.829 s	5.832 s	5.890 s	6.726 s (too late)

where θ_1 is not known. The idea of the GLR algorithm is to use, for each point of the signal (k values), the value of θ_1 that maximizes $S_j^k(\theta_1)$; the decision rule is given by

$$t_a = \min[k | \max_{1 \le j \le k} \sup_{\theta_1} S_j^k(\theta_1) \ge h] \tag{20}$$

Not all probability densities allow this maximization (the conditions that are to be fulfilled can be found in [29]); in particular, $p_\theta(x)$ should belong to the so-called Koopman–Darmois family:

$$p_\theta(x) = e^{\theta T(x) - d(\theta)} h(x) \tag{21}$$

where d is strictly concave upward and infinitely differentiable over an interval of the real line. It is possible to write a Gaussian distribution under this form, assuming

$$T(x) = \frac{-(x-\mu)^2}{2}, \qquad d(\theta) = -\ln(\sqrt{\theta}), \qquad h(x) = \frac{1}{\sqrt{2\pi}}$$

where μ is the mean and the parameter θ is the inverse of the variance $\theta = 1/\sigma^2$.

Then one can prove that $S_j^k(\theta_1)$ is maximized with

$$\theta_1 = \frac{k-j+1}{\sum_{i=j}^k (x_i - \mu)^2}$$

One finally obtains

$$\sup_{\theta_1} S_j^k(\theta_1) = (k-j+1)\left[\ln\left(\sqrt{\frac{k-j+1}{\sum_{i=j}^k (x_i-\mu)^2}}\right) - \ln(\sqrt{\theta_0}) - \frac{1}{2}\right] + \frac{\theta_0}{2}\sum_{i=j}^k (x_i - \mu)^2 \tag{22}$$

where $\theta_0 = 1/\sigma_0^2$, the inverse of the variance before change.

The GLR algorithm gives the alarm if $\max_{1 \le j \le k} \sup_{\theta_1} S_j^k(\theta_1) \ge h$, where h is a user-defined threshold. This double maximization ensures that any change will be detected, even if the PDF after change is unknown: by always choosing the highest possible value of $S_j^k(\theta_1)$, we maximize the chance to detect it. However, its disadvantage is that it makes the algorithm very time- and memory-consuming. Indeed, at every time step k, all values of $\sup_{\theta_1} S_j^k(\theta_1)$ for j between 1 and k have to be calculated and compared with each other. This may make its implementation on an online-embedded data processing device more difficult.

2. *Application to Buzz Detection*

The GLR algorithm was applied to the signal already presented in Sec. IV.B.2. The PDF before change was also estimated to be between $t = 2$ and 2.5 s. Figure 15 shows this signal and the evolution of $g_k = \max_{1 \le j \le k} \sup_{\theta_1} S_j^k(\theta_1)$. With a value of threshold $h = 100$, the alarm is given at time $t = 2.577$ s and buzz starts at $t = 2.78$ s.

When applied to a real signal, the GLR algorithm meets the same issues as the CUSUM algorithm: $p_0(x)$ is not known and has to be estimated online, and the analyzed signal has to be centered on zero and filtered to get rid of the variations of mean and high-frequency noise. So the algorithm has to be adapted in the same way as the CUSUM algorithm, as already described in Sec. IV.B.3.

Once these adaptations have been made, one can test the GLR algorithm in real conditions on a more complex signal (for instance, the signal recorded by sensor K6 at $M = 2$ with bleed, which was already presented in Sec. IV.B.3; Fig. 16 shows this signal, the evolution of g_k, and the alarm time). The intermediate steps (zero-mean filtered signal and calculation of σ_0) are the same as in Fig. 14.

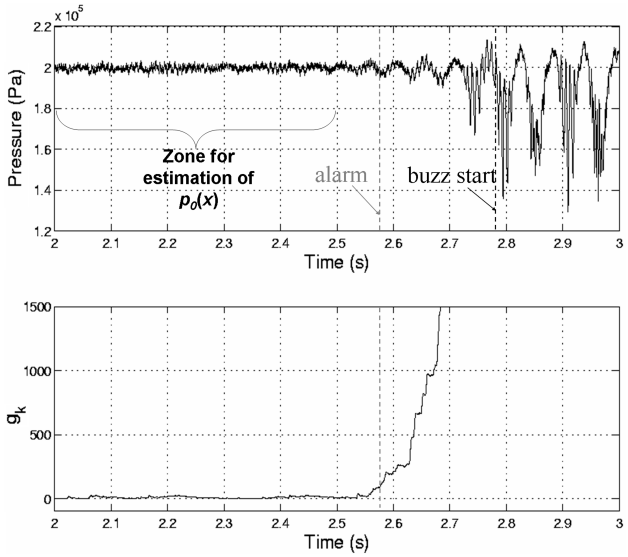

Fig. 15 Detection of the signal PS33 divergence at $M = 1.8$ by the GLR algorithm.

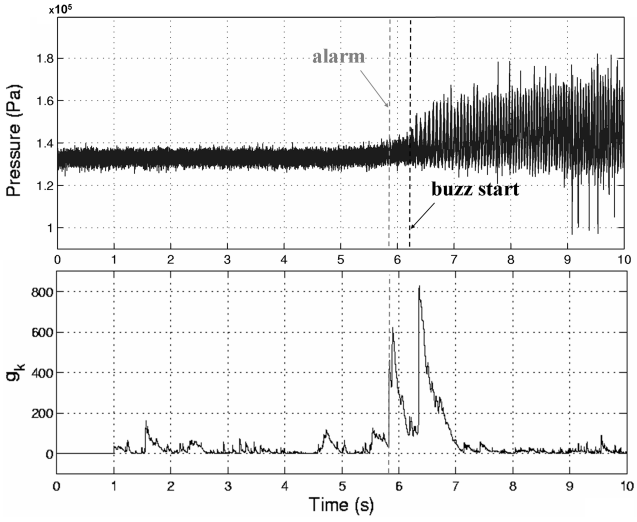

Fig. 16 Detection of the big buzz onset on signal K6, at $M = 2$ with bleed by the GLR algorithm.

With a threshold value of $h = 400$, the alarm is given at $t = 5.825$ s, almost at the same time as by the CUSUM algorithm. The graph of g_k shows two noticeable peaks: the first one corresponds to the beginning of the divergence of buzz frequency that must be detected, and the second one corresponds to the strong oscillations of buzz.

Finally, the adapted versions of the CUSUM and GLR algorithms give rather similar results: both allow detecting buzz onset more than one tenth of a second before it starts. The advantage of the GLR algorithm is that it needs only one parameter (threshold h), instead of the two needed for the CUSUM algorithm (h and K), which makes it more general and simpler to use. But its main disadvantage is its cost in terms of memory and calculating time, which is much higher than that for the CUSUM algorithm and could make its practical implementation difficult on an embedded device.

D. Practical Issues

This section deals with some practical issues related to the use of change-detection algorithms for the detection of buzz onset. A first point is the location of the appropriate pressure sensor for supplying the analyzed signal. Experiments show that the signals on which buzz precursors appear the most clearly (and are therefore easier to

detect) are those recorded by sensors located just downstream of the normal shock before buzz starts: that is where pressure fluctuations are the strongest, and the sensor used for detection should ideally be located there. However, the normal shock position is not constant and depends on the Mach number, and so a sensor located just downstream of the shock for a particular Mach number will be in a supersonic zone (and so will become useless) for a greater Mach number. It means that several sensors located in different points of the inlet would be needed, and the algorithm should switch from one to another, depending on the flight conditions. A simpler solution would consist of using a sensor located in the diffuser, behind the most downstream position of the shock, so that it is always located in a subsonic zone. According to our experience, the pressure fluctuations at this location, although weaker than just downstream of the shock, are sufficient to detect buzz onset early enough.

A second point is the acquisition frequency of the signals. A high frequency is, of course, desirable because it gives better performances to the algorithm. However, it also means more points to be analyzed (so a higher calculating time). Our sensors' frequency was 10 kHz, but tests have shown that a frequency of 2 kHz (i.e., 1000 times the frequency of the big buzz) still gave acceptable results.

V. Conclusions

Supersonic inlet buzz was studied on a rectangular mixed-compression inlet model at Mach numbers 1.8 and 2. Two kinds of buzz have been observed: the big buzz (low frequency, triggered by a separation on the compression ramps), which occurred in all cases, and the little buzz (higher frequency, triggered by the presence of shear layers under the cowl lip), which occurred at Mach 2 before the onset of the big buzz. Note that the little buzz can be suppressed by a boundary-layer bleed device.

We examined the pressure signals recorded when buzz started. These signals are nonstationary in a statistical sense, and so the classical signal-processing tools (such as the Fourier transform, which does not take into account any evolution in time) are not relevant. We used time–frequency signal-processing tools such as the spectrogram, wavelet transform, and Wigner–Ville distribution. Wavelet transform appeared particularly efficient in our case (in particular, for low frequencies), due to its adaptable resolution. These tools allowed us to study the evolution in time of the energy levels corresponding to buzz frequencies. We noticed, in particular, that at Mach 2, at the transition between the little buzz and the big buzz, the energy seemed to switch from one frequency to the other, with the total energy remaining constant. We also noticed that in every one of our experimental cases, the energy level at the frequency of the big buzz (18 Hz) increased progressively over several tenths of seconds, before the very start of the big buzz itself. This occurred even while the little buzz (when existing) was still prevailing. If this increase in the energy level could be detected early enough before the big buzz onset, a control device could be automatically activated to avoid buzz.

Two change-detection algorithms based on a statistical rule of decision were tested on our signals: the CUSUM and GLR algorithms; both provided similar results and were able to detect buzz early enough before its onset. However, the GLR algorithm, although simpler to use because it does not require the knowledge of the signal properties after change, appears to be difficult to use online because of its high demands in calculation time.

Finally, it was shown that the inlet buzz phenomenon can be detected in advance, which could make it possible to avoid buzz with the use of a control device. However, the detection algorithm, whichever it is, must have its parameter(s) adjusted; for that purpose, a preliminary wind-tunnel experimental study of the inlet is probably necessary.

Acknowledgments

The authors are grateful to L. Daudet (Laboratoire d'Acoustique Musicale/Paris 6) for fruitful discussions on signal processing and change detection. J. M. Massonat (ONERA/Centre de Modane–Avrieux), who conducted the experiments, is also acknowledged.

References

[1] Ferri, A., and Nucci, L. M., "The Origin of Aerodynamic Instability of Supersonic Inlets at Subcritical Conditions," NACA RM L50K30, 1951.

[2] Dailey, C. L., "Supersonic Diffuser Instability," Ph.D. Thesis, California Inst. of Technology, Pasadena, CA, 1954.

[3] Trimpi, R., "A Theory for Stability and Buzz Pulsation Amplitude in Ram Jets and an Experimental Investigation Including Scale Effects," NACA Rept. 1265, 1956.

[4] Fisher, S. A., Neale, M. C., and Brooks, A. J., "On the Sub-Critical Stability of Variable Ramp Intakes at Mach Numbers Around 2," National Gas Turbine Establishment, Rept. ARC-R/M-3711, Fleet, England, U.K., Feb. 1970.

[5] Nagashima, T., Obokata, T., and Asanuma, T., "Experiment of Supersonic Air Intake Buzz," Inst. of Space and Aeronautical Science, Rept. 481, Tokyo, Nov. 1972.

[6] Oswatitsch, K., "Der Druckrückgewinn bei Geschossen mit Rückstossantrieb bei Hohen Übershallgeschwindigkeiten (Der Wirkungsgrad vos Stossdiffusoren)," Forschungen und Entwicklungen des Heereswaffenamtes, Rept. 1005, Göttingen, Germany, 1944; also "Pressure Recovery for Missiles with Reaction Propulsion at High Supersonic Speeds (The Efficiency of Shock Diffusers)," NACA TM-1140, 1947 (in English).

[7] Sterbentz, W., and Evvard, J., "Criterions for Prediction and Control of Ram-Jet Flow Pulsations," NACA RM E51C27, 1951.

[8] Leynaert, J., "Une Description Globale Élémentaire du Pompage des Prises d'Air Supersoniques," ONERA Rept. 47/2149 A, Châtillon, France, 1968.

[9] Leynaert, J., "Pompage dans les Entrées d'Air Supersoniques," *L'Aéronautique et l'Astronautique*, Vol. 22, No. 6, 1970, pp. 47–62.

[10] Newsome, R., "Numerical Simulation of Near-Critical and Unsteady, Subcritical Inlet Flow," *AIAA Journal*, Vol. 22, No. 10, 1984, pp. 1375–1379.

[11] Lu, P.-J., and Jain, L.-T., "Numerical Investigation of Inlet Buzz Flow," *Journal of Propulsion and Power*, Vol. 14, No. 1, Jan.–Feb. 1998, pp. 90–100.

[12] Trapier, S., Duveau, P., and Deck, S., "Experimental Study of Supersonic Inlet Buzz," *AIAA Journal*, Vol. 44, No. 10, 2006, pp. 2354–2365.

[13] Cole, G. L., Neiner, G. H., and Wallhagen, R. E., "Coupled Supersonic Inlet-Engine Control Using Overboard Bypass Doors and Engine Speed to Control Normal Shock Position," NASA TN D-6019, Dec. 1970.

[14] Watanabe, Y., and Murakami, A., "Control of Supersonic Inlet with Variable Ramp," 25th Congress of the International Council of the Aeronautical Sciences, International Council of the Aeronautical Sciences Paper ICAS-2006-5.2.4, 2006.

[15] Lee, I., and Sung, H. J., "Characteristics of Wall Pressure Fluctuations in Separated and Reattaching Flows over a Backward-Facing Step," *Experiments in Fluids*, Vol. 30, No. 3, 2001, pp. 262–282.

[16] Feron, E., Brenner, M., Paduano, J., and Turevskiy, A., "Time-Frequency Analysis for Transfer Function Estimation and Applications to Flutter Clearance," *Journal of Guidance, Control, and Dynamics*, Vol. 21, No. 3, May–June 1998, pp. 375–382.

[17] Jeng, Y. N., Chen, C. T., and Cheng, Y. C., "Some Detailed Information of a Low Speed Turbulent Flow over a Bluff Body Evaluated by New Time-Frequency Analysis," AIAA Paper 2006-3340, 2006.

[18] Farge, M., "Wavelet Transforms and Their Applications to Turbulence," *Annual Review of Fluid Mechanics*, Vol. 24, 1992, pp. 395–457.

[19] Fröhlich, J., "LES of Vortex Shedding Past Circular Cylinders," *Proceedings of ECOMAS 2000* [CD-ROM], International Center for Numerical Methods in Engineering (CIMNE), Barcelona, Spain, 2000.

[20] Flandrin, P., *Temps-Fréquence*, Editions Hermès, Paris, 1993.

[21] Mallat, S., *Une Exploration des Signaux en Ondelettes*, Editions de L'Ecole Polytechnique, Paris, 2000.

[22] Mallat, S., *A Wavelet Tour of Signal Processing*, Academic Press, New York, 1999.

[23] Hammond, J. K., and White, P. R., "The Analysis of Non-Stationary Signals Using Time-Frequency Methods," *Journal of Sound and Vibration*, Vol. 190, No. 3, 1996, pp. 419–447.

[24] Mevel, L., Basseville, M., and Benveniste, A., "Fast In-Flight Detection of Flutter Onset—A Statistical Approach," Inst. de Recherche en Informatique et Systèmes Aléatoires (IRISA), Rept. 1541, Rennes,

France, Oct. 2003.
[25] Girault, J. M., "Apport des Techniques du Traitement du Signal à l'Analyse et Détection de Signaux Emboliques," Ph.D. Thesis, Univ. de Tours, Tours, France, Dec. 1999.
[26] Basseville, M., and Nikiforov, I. V., *Detection of Abrupt Changes: Theory and Application*, Prentice–Hall Information and System Science Series, Prentice–Hall, Englewood Cliffs, NJ, 1993; also available at http://www.irisa.fr/sisthem/kniga/kniga.pdf.
[27] Bendat, J. S., and Piersol, A. G., *Random Data: Analysis and Measurement Procedures*, Wiley-Interscience, New York, 1971.
[28] Page, E. S., "Continuous Inspection Schemes," *Biometrika*, Vol. 41, 1954, pp. 100–115.
[29] Lorden, G., "Procedures for Reacting to a Change in Distribution," *Annals of Mathematical Statistics*, Vol. 42, No. 6, 1971, pp. 1897–1908.

D. Gaitonde
Associate Editor